Photoluminescence from C_{60}-coupled porous structures formed on Fe^+-implanted silicon

Z. Y. Zhang, X. L. Wu,[a] and T. Qiu
National Laboratory of Solid State Microstructures, Department of Physics, Nanjing University, Nanjing 210093, People's Republic of China

P. Chen, Paul K. Chu, and G. G. Siu
Department of Physics and Materials Science, City University of Hong Kong, Kowloon, Hong Kong

D. L. Tang
Southwestern Institute of Physics, Chengdu 610041, People's Republic of China

(Received 15 February 2006; accepted 16 May 2006; published online 5 July 2006)

⟨111⟩-oriented *p*-type Si wafer with a resistivity of 1–5 Ω cm was implanted with Fe^+ and then annealed at 1100 °C in N_2 for 60 min, followed by anodization in a solution of HF to form porous structure with β-$FeSi_2$ nanocrystallites. Photoluminescence (PL) spectral measurements show that a strong PL peak appears in the range of 610–670 nm. The position of the PL peak remains unchanged, but its intensity increases with the storage time in air until about three months and then saturates. C_{60} molecules were chemically coupled on the porous structure through a kind of silane coupling agent to form a nanocomposite. It is revealed that the stable PL peak monotonically shifts to a pinning wavelength at 570 nm. Experimental results from PL, PL excitation, Raman scattering, and x-ray diffraction measurements clearly show that the pinned PL originates from optical transition in C_{60}-related defect states, whereas the photoexcited carriers occur in the β-$FeSi_2$ nanocrystallites formed during anodization. This work opens a new way to tailor nanometer environment for seeking optimal luminescent properties. © *2006 American Institute of Physics*. [DOI: 10.1063/1.2212408]

I. INTRODUCTION

Since the discovery of porous silicon (PS) with visible emission at room temperature,[1] light-emitting properties of silicon-based semiconductor nanomaterials have attracted more attention and have been investigated widely.[2–11] Due to instabilities of the structural and light-emitting properties of porous silicon, obtaining strong and stable light emission has become a subject of many experimental investigations. For PS, many experiments have demonstrated that its luminescence property is not only determined by the quantum confinement effect of Si nanocrystals but also controlled by the surface chemical bonds.[8–14] Both the surface layer and nc-Si core constitute a nanoparticle composite. Naturally, its luminescence is a result of the interaction of the two nanoparticles. This kind of nanocomposite generally exists in luminescent semiconductor nanostructures. Thus, studies on the light-emitting properties of nanocomposites will be a basis for improving the luminescence efficiency and stability. To reach the purpose, many investigators have fabricated the PS structures with various surface passivations such as Fe,[15,16] Au,[17] and oxygen (Refs. 18 and 19) and revealed the influence of surface chemical bonds on photoluminescence (PL) properties.[8–10] The improvements of the intensity and stability have been observed. To further tailor the nanometer environment, a significant work is to couple C_{60} molecules at the surfaces of PS nanocrystals to form a composite nanostructure. We know that C_{60} molecule has a highly symmetrical structure and unique physical and chemical properties,[20] but it can only emit a weak PL in the red at room temperature. It has been shown that if C_{60} molecules are placed in certain environments, the PL intensity related to C_{60} can greatly be improved.[21,22] Different matrices will lead to different optical characteristics of C_{60} due to the quantum confined geometry and host/guest interaction. Therefore, the C_{60}/PS nanocomposite can be expected to have new light-emitting features.[13,23]

In this work, we first fabricate a kind of porous structure with β-$FeSi_2$ nanocrystals by anodization of Fe^+-implanted silicon and then couple C_{60} molecules to the surface of the porous structure. Microstructural analyses indicate that α- and β-$FeSi_2$ nanocrystals are initially formed during high temperature annealing of Fe^+-implanted silicon. Subsequent anodization leads to the disappearance of original α- and β-$FeSi_2$ components and the formation of a new textured β-$FeSi_2$ component together with Si nanocrystallites. For the porous structure coupled with C_{60}, the obtained PL spectra display a pinning wavelength at 570 nm, instead of the 610–670 nm PL peaks which possibly arise from the quantum confinement on Si nanocrystals in the porous structure without C_{60} coupling, based on our experimental results. PL excitation (PLE) spectral analyses illustrate that the pinning PL peak originates from optical transition in C_{60}-related defect states, but the photoexcited carriers occur in the

[a]Author to whom correspondence should be addressed. Electronic mail: hkxlwu@nju.edu.cn

β-$FeSi_2$ nanocrystals. This work opens a new way to tailor nanometer environment for optimization of luminescent properties.

II. SAMPLES AND EXPERIMENTS

⟨111⟩-oriented *p*-type silicon wafer with a resistivity of 1–5 Ω cm was implanted with Fe ions at a dose of 3×10^{17} cm^{-2} and an energy of 120 keV. The implanted silicon wafer was then annealed in N_2 at 110 °C for 60 min, followed by anodization in a solution of ethanol:HF=1:2 (99.7% C_2H_5OH: 40% HF) to form porous structure. The anodic process was carried out in the dark for 20 min. Three typical samples (marked as A, B, and C) were obtained with the etching current densities of 30, 20, and 10 mA/cm^2, respectively. This kind of porous structural samples is called as FePS. The fresh FePS samples show a strong PL peak in the 610–670 nm range under our experimental conditions. After they were exposed in air, their PL positions remain unchanged, but their intensities increase with the storage time in air and reach saturation three months later.

Each FePS sample with a saturated PL peak was subsequently cut into four pieces to identify the influence of various postprocessing conditions on the PL properties. The first one was considered as original FePS (samples A1, B1, and C1). The second one was chemically coupled with C_{60} molecules and thus considered as C60FePS (samples A2, B2, and C2). The third one was treated with the same process like the second one, but the reflux step was carried out in a pure toluene solution without C_{60} (samples A3, B3, and C3). The fourth one was chemically coupled with C_{60} molecules like the second one and then was annealed in N_2 at 400 °C for 30 min (samples A4, B4, and C4). The C_{60}-coupled experiments are described as follows. (1) The FePS samples were immersed in a mixture of NH_3 (25%), H_2O_2 (30%), and de-ionized water with a volume ratio of 1:1:5 at a temperature of 70 °C for 20 min. The FePS samples were subsequently taken out to be washed with de-ionized water and dried in a stream of N_2. (2) The treated FePS samples were then immersed in a solution of 3-(diethoxymethylislyl)-propylamine $[(C_2H_5O)_2Si(CH_3)(CH_2)_3NH_2]$ (1 wt %) with toluene at 60±1 °C for 4 min. The resultant FePS samples were washed repeatedly with toluene and dried with a stream of N_2.[24] This process makes the coupling agent coupled on the surface of the oxidized FePS. (3) The FePS samples with the coupling agent were immersed in a 0.2 mmol/l toluene solution of C_{60} powder (>99.9%) and refluxed at a temperature of 120 °C for 60 min. The final products were washed with toluene to remove free uncombined C_{60} molecules and dried in a stream of N_2 to form the C60FePS samples. In our experiments, PL and PLE measurements were carried out on a Hitachi 850 fluorescence spectrophotometer. High-resolution transmission electron microscope (HRTEM) images were taken on an FEI Tecnai G^2 20 S-TWIN TEM. Raman spectra were obtained on a T64000 triple Raman system. X-ray diffraction (XRD) spectra were taken on a Rigaku 3015 type single crystal diffractometer using Cu $K\alpha$ radiation. The wavelength of x ray is 0.154 nm. All the measurements were performed at room temperature.

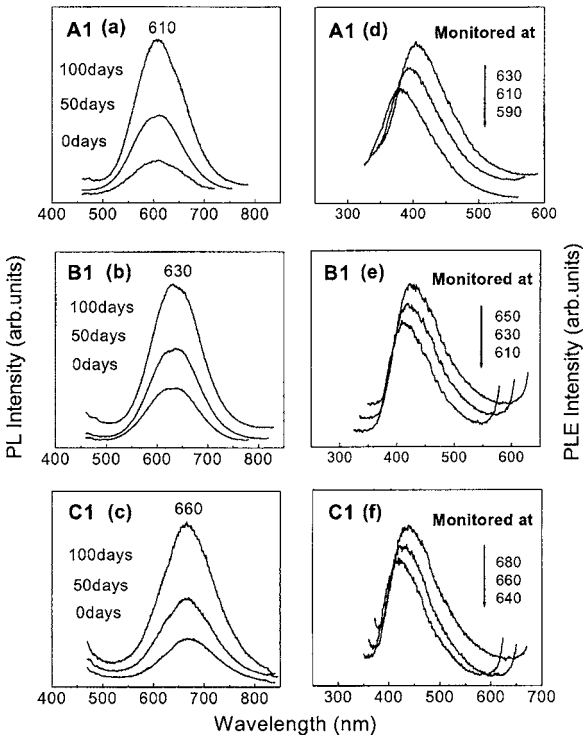

FIG. 1. (a)–(c) PL spectra of samples A1, B1, and C1 stored in air for 0, 50, and 100 days, respectively. (d)–(f) PLE spectra of samples A1, B1, and C1 taken under three monitoring wavelengths.

III. RESULTS AND DISCUSSIONS

Figure 1 shows the PL and PLE spectra of samples A1, B1, and C1. The PL peaks of the three fresh FePS samples are localized at 610, 630, and 660 nm, respectively. After these samples are stored in air, their PL peak positions remain unchanged, but their PL intensities increase monotonically with the storage time and reach saturation three months later [Figs. 1(a)–1(c)]. The PLE spectra of all the FePS samples show a strong PLE peak with a large Stokes shift of ~1.1 eV. A sharp feature of these PLE spectra is that the position of the PLE peak redshifts with increasing the monitoring wavelength, as shown in Figs. 1(d)–1(f). This result suggests that the PLE peak should originate from a special excitation in the band with quantum confinement.[23,25] This viewpoint may cause an argument. In the hybrid polyatomic surface-coupled fluorophore model,[26] the PLE spectral shift with the monitoring wavelength was also observed and related to the surface fluorophore. However, a careful comparison may find that the two kinds of PLE spectra are completely different in shape. Our PLE spectra have a peaklike shape[25,27] and its shift with the monitoring wavelength indicates its dependence on Si crystallite size distribution,[28] while the PLE spectra connected with the surface fluorophore show an absorption edge, similar to that in bulk Si. Thus, the excitation process of carriers in our experiments should take place in the cores of Si nanocrystals with different band gaps depending on the crystallite sizes. After these FePS samples were coupled with C_{60} (A2, B2, and C2), the PL peak intensities slightly change, but the peak positions monotonically shift to 570 nm [Figs. 2(a)–2(c)]. PLE spectral examinations further found that the PLE peak positions

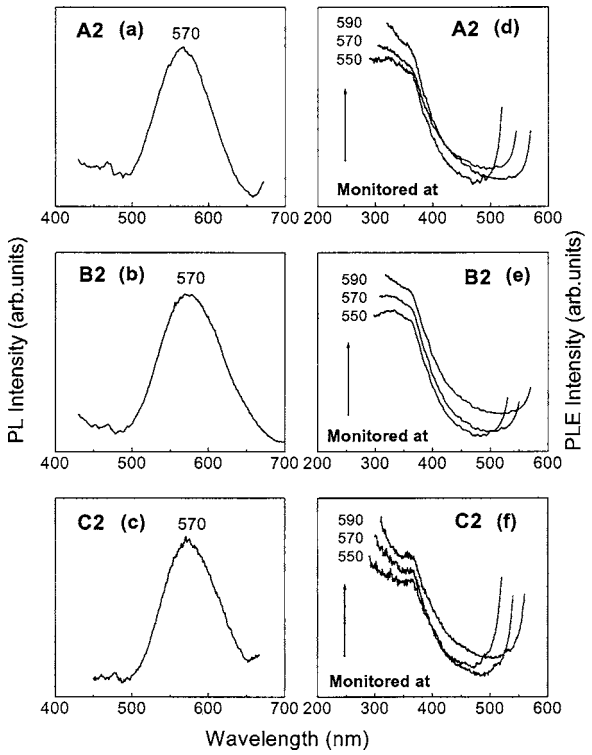

FIG. 2. (a)–(c) PL spectra of samples A2, B2, and C2, respectively. (d)–(f) PLE spectra of samples A2, B2, and C2, respectively taken under three monitoring wavelengths.

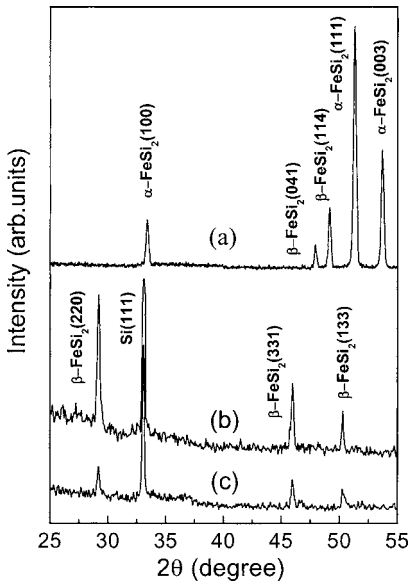

FIG. 3. XRD patterns of (a) Fe^+-implanted silicon wafer annealed in N_2 at 1100 °C for 60 min, (b) sample A1 (B1 or C1), and (c) sample A2 (B2 or C2).

are pinned at 370 nm under different monitoring wavelengths [Figs. 2(d)–2(f)] and remain unchanged with increasing the storage time in air. From the difference in PLE spectra between FePS and C60FePS, we can infer that their light-emitting mechanisms are different.

Previously, we have known that usual PS sample exhibits a PL intensity degradation after exposed to air, accompanied with a blueshift or redshift of the peak position.[12,13] By comparing the XRD spectrum of the Fe^+-implanted silicon wafer [Fig. 3(a)] with that of the FePS sample [Fig. 3(b)], we may find that some new β-$FeSi_2$ nanocrystals with orientations different from those in the Fe^+-implanted silicon wafer have been formed together with Si nanocrystallites in process of electrochemical etching. To identify the existence of β-$FeSi_2$ and Si nanocrystals, we immersed the FePS sample in an ultrasound water bath. This makes the top layer of the sample, a weakly interconnected nanostructure network, partially crumbled and dispersed in ethanol solution. The HR-TEM image can be obtained by dripping the crumbled nanocrystal suspension on a graphite grid. A typical image is shown Fig. 4. It can be seen that the FePS sample contains both the β-$FeSi_2$ and Si nanocrystals and especially, two small-size β-$FeSi_2$ nanocrystals were observed to exist at the surface of a large-size Si nanocrystal. As reported previously,[15] such samples are easily passivated by some Fe–O bonds to form a thin Fe_2O_3 layer possibly around the β-$FeSi_2$ nanocrystal when they are stored in air. With increasing the storage time, the Fe_2O_3 layer will thicken as a result of the increase of the Fe–O bond density.[15] If considering the presence of a transition region between the β-$FeSi_2$ and Fe_2O_3 layers and its thinning caused by its storage in air, we found that the band-mixing model,[14] which can give the energy levels of electrons and holes confined in the $Si/FeSi_2$ nanocomposite consisting of nanocrystalline Si core, interfacial $FeSi_2$ layer, and outer Fe_2O_3 crust, can explain very well the observed PL intensity increase with the sample storage time and the pinning behavior of the PL peak position. This implies that the PL behavior from the FePS samples is related to both the quantum confinement of Si nanocrystal and its surface passivation (the formation of Fe–Si and Fe–O bonds). Here we would like to mention that in the hybrid polyatom surface-coupled fluorophore model,[26] the PL spectral distributions of aqueous etched PS are independent of the choice of sample preparation parameters, and while samples may show somewhat different PL spectral distributions shortly after they have been produced, when stored in air at room temperature, they slowly change to a steady state or equilibrated distribution after aging for periods of a few months.[26] From the PL spectra in our experiments [Figs. 1(a)–1(c)], we can see that the PL spectral distributions strongly correlate with the selected etching parameters. When the samples were stored in air, the PL peak positions

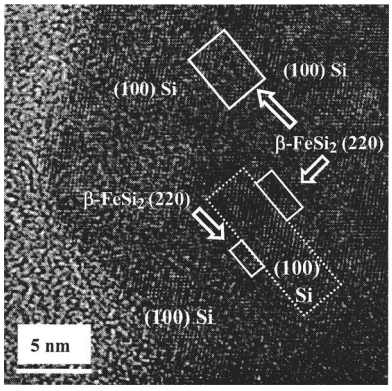

FIG. 4. A typical HRTEM image of the FePS samples.

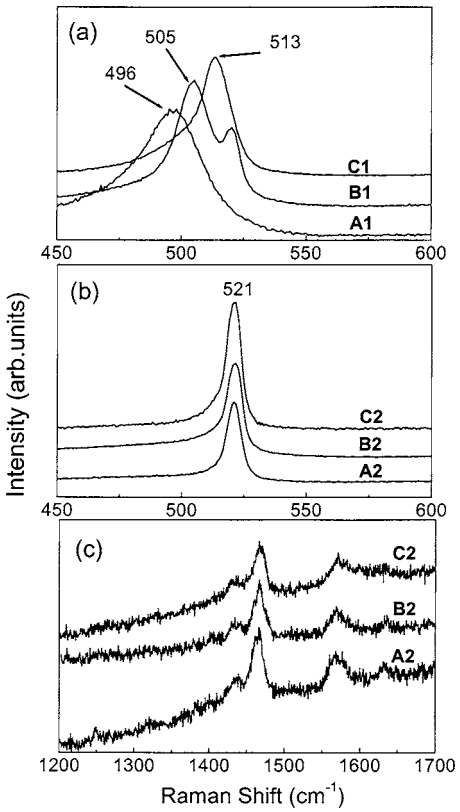

FIG. 5. Raman spectra of (a) samples A1, B1, and C1 in the wave number range of 450–600 cm^{-1}, (b) samples A2, B2, and C2 in the wave number range of 450–600 cm^{-1}, and (c) samples A2, B2, and C2 in the wave number range of 1200–1700 cm^{-1}.

remain unchanged but their intensities increase monotonically with the storage time and reach saturation three months later. So we consider the observed phenomena not to be due to the hybrid polyatom surface-coupled fluorophore. To further identify the origin of the PL peak, we examined the Raman spectra of samples A1, B1, and C1 and present the corresponding results in Fig. 5(a). The three spectra all display asymmetrical broad peaks at 496, 505, and 513 cm^{-1}, respectively. According to Scherrer's formula,[29] we can estimate the mean Si crystallite sizes to be 1.5–3.0 nm. Such Si nanocrystallites will have a widened band gap in the range of 520–700 nm based on the calculations from the quantum confinement model.[12,13] Therefore, we can accept the PL peak in the wavelength range of 610–670 nm to be related to the Si nanocrystals and their surface passivation.

The above-noted assignment may cause another suspicion, that is, whether the 610–670 nm PL is due to the band to band recombination in the quantum confined β-$FeSi_2$ nanocrystallites. This seems to be possible because some new β-$FeSi_2$ nanocrystallites have been formed in the FePS samples. Generally, it was accepted that β-$FeSi_2$ is a direct gap semiconductor with band gap of about 0.85 eV,[30,31] but some calculations show that β-$FeSi_2$ is also an indirect gap semiconductor with band gap of about 0.80 eV at room temperature.[32,33] When bulk β-$FeSi_2$ becomes nanocrystallite, its band gap would widen and possibly reach the observed PL peak energy owing to the quantum confinement effect. To rule out this suspicion, we examined the XRD spectra of C60FePS samples and a typical result is presented in Fig. 3(c). We can see that when C_{60} is coupled to the FePS sample, the β-$FeSi_2$ component still exists. Only the intensities of diffraction peaks are reduced. Corresponding to disappearance of the 610–670 nm PL peak and change of the PLE peak behavior, we can reasonably infer that the radiation from the FePS samples is not due to the quantum confinement on the β-$FeSi_2$ nanocrystallites.

From the above analyses, we can see that the pinning 570 nm PL in the C60FePS samples has an origin different from the 610–670 nm PL in the FePS samples. To clarify its mechanism, we examined the Raman spectra of the C60FePS samples. From our treatment on the C60FePS samples, it can be inferred that C_{60} molecules should completely be coupled to the FePS sample and no free C_{60} molecules exist at the sample surface. This can let us identify whether the photoexcited carriers are from the coupled C_{60} molecules by examining the Raman peak positions. Figures 5(b) and 5(c) present a typical Raman scattering result in the spectral ranges of 450–600 and 1200–1700 cm^{-1}, respectively. For the Raman spectral range of 400–600 cm^{-1}, we can only observe a narrow Raman peak at 521 cm^{-1}. Evidently, the asymmetrical broad Raman peak connected with nanocrystalline Si has vanished. The obtained Raman signal at 521 cm^{-1} is mainly the contribution from Si substrate. The disappearance of Si nanocrystallites was also found in the FePS samples only with a reflux processing, indicating that the surface oxidization caused by hot reflux is responsible for the disappearance of Si nanocrystallites. This result means that the 570 nm PL has nothing to do with Si nanocrystallites. In the 1200–1700 cm^{-1} region, three characteristic phonon modes connected with C_{60} molecules can be observed at 1428(H_g), 1468(A_g), and 1570 cm^{-1}(H_g).[34,35] The 1468 cm^{-1} vibration mode is well known to be very sensitive to intermolecular bonding and closely related to charge transfer in the corresponding PL spectra.[36] As we have known, C_{60} can only emit a weak PL at 730 nm.[13] Thus, if the coupled C_{60} molecules could provide the photoexcited carriers to radiatively recombine in the interfacial defect states, a shift of the Raman mode at 1468 cm^{-1} can really be expected. However, no obvious $A_g(2)$ mode shift was observed in comparison with the standard value of 1468–1470 cm^{-1}.[37,38] This implies that the coupled C_{60} does not provide any carriers for the radiation at 570 nm.

Since the reflux treatment and C_{60} coupling make the FePS become the C60FePS, C_{60} molecules or coupling agent-related defects may be the origin of the 570 nm PL. According to this inference, we examined the PL spectra of samples A3, B3, and C3 to check the influence of the coupling agent. A typical result is presented in Fig. 6(a). It can be seen that no PL peak exists in the spectrum, indicating that the coupled C_{60} is an important factor for causing the pinning PL. The radiative defect centers should be localized at the coupling agent/C_{60} interface. Correspondingly, the 570 nm PL arises from the interfacial binding states between the coupling agent and C_{60}. To confirm this point, we annealed the C60FePS samples at 400 °C in N_2 for 30 min to form samples A4, B4, and C4. The coupling agent should be pyrolyzed at 400 °C. We found that the PL spectra from

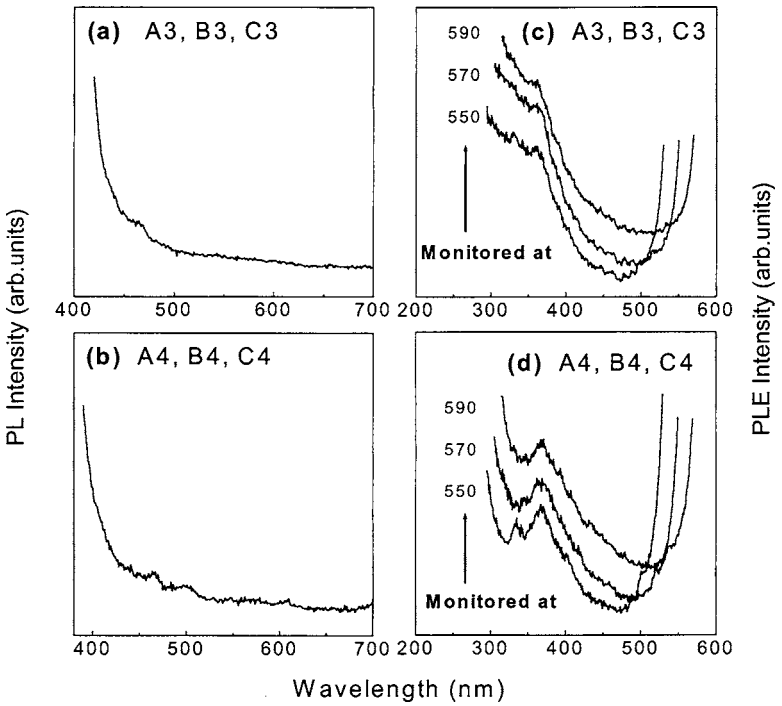

FIG. 6. PL spectra of (a) sample A3 (B3 or C3) and (b) sample A4 (B4 or C4) taken under excitation with the 370 nm line of a Xe lamp. PLE spectra of (c) sample A3 (B3 or C3) and (d) sample A4 (B4 or C4) taken under three monitoring wavelengths.

samples A4, B4, and C4 show no any PL peak in the measured range [a typical PL spectrum is illustrated in Fig. 6(b)]. This indicates that the coupling agent is really also an important factor for causing the 570 nm PL. It is both the coupling agent and C_{60} that commonly determine the pinning PL.

The excitation process of carriers for the radiation at 570 nm is interesting. In Figs. 2(d)–2(f), we have seen that the 570 nm PL has a characteristic PLE peak at 370 nm. This PLE peak position keeps unchanged with the monitoring wavelength. To identify the origin of the PLE peak, we examined the PLE spectra of samples A3, B3, and C3 without C_{60} coupling. We found that the PLE spectra of the three samples are similar to those of samples A2, B2, and C2, with all displaying a pinning PLE peak at 370 nm. Its position remains unchanged with the monitoring wavelength [see Fig. 6(c)]. This result suggests that the photoexcited carriers are not from the coupled C_{60} molecules, but relate to the composite of the coupling agent and β-$FeSi_2$. Further, we examined the PLE spectra of samples A4, B4, and C4 and found that all the PLE spectra are also identical to those of the FePS samples, as shown in Fig. 6(d). This result implies that the coupling agent is not also an origin for producing the photoexcited carriers. Since the surfaces of samples A4, B4, and C4 are completely different from those of samples A3, B3, and C3 (the pyrolysis of the coupling agent will largely change the surface structure of β-$FeSi_2$ nanocrystallites), the coupling agent/β-$FeSi_2$ nanocrystallite interface is not also responsible for the pinning 370 nm PLE spectra. Considering the PLE properties and structural features of all the samples, a possible origin of the photoexcited carriers can be presented: the photoexcited carriers are related to the β-$FeSi_2$ nanocrystallites. According to the quantum confinement model, the band gap of $FeSi_2$ will widen when its size is reduced to nanometer scale and meanwhile the excitation efficiency will greatly be increased. In our current samples, the β-$FeSi_2$ nanocrystallites should be rather small and almost uniform in size. This can roughly be inferred from the XRD result [Fig. 3(c)]. Thus, a pinning PLE spectral feature is understandable. To further seek the argument for the origin of the pinning PLE peak, we made a series of contrastive experiments using *c*-Si, B^+-implanted, P^+-implanted, and C^+-implanted Si wafers. We used completely the same experimental conditions to form the C_{60}-coupled PS samples. We found that no similar PLE spectra were observed. So we can reasonably infer that the photogeneration of carriers for producing the 570 nm PL occurs in the $FeSi_2$ nanocrystallites, whereas their radiative recombination takes place at the interfacial binding states between the coupling agent and C_{60}.

IV. CONCLUSIONS

We have revealed two kinds of light-emitting mechanisms in the FePS and C60FePS samples. For the FePS samples, the PL peak positions remain unchanged, but their intensities increase with the storage time in air and reach saturation three months later. Spectral analyses suggest that the PL from the FePS samples originates from the quantum confinement on Si nanocrystallites. Stable Fe–Si bonds at the surfaces of Si nanocrystallites protect Si cores from oxidization in air and therefore keep their sizes unvaried. Meantime, Fe^+ passivations remove residual Si dangling bonds and thus keep the stability of the PL intensity. For the C_{60}-coupled FePS samples, the PL peaks shift to a pinning wavelength at 570 nm. Our experimental results clearly show that the photoexcited carriers occur in the quantum confined β-$FeSi_2$ nanocrystallites, whereas the radiation at 570 nm takes place at the interfacial binding states between the coupling agent and C_{60}.

ACKNOWLEDGMENTS

This work was supported by the grants (Nos. 10225416, 60476038, and 60576061) from the National Natural Science Foundation of China and the LAPEM. Partial support was also from the Major State Basic Research Project No. G001CB3095 of China and City University of Hong Kong Direct Allocation Grant No. 9360110.

[1] L. T. Canham, Appl. Phys. Lett. **57**, 1046 (1990).
[2] *Porous Silicon*, edited by Z. C. Feng and R. Tsu (World Scientific, Singapore, 1994).
[3] K. D. Hirschman, L. Tsybeskov, S. P. Duttagupta, and P. M. Fauchet, Nature (London) **384**, 338 (1996).
[4] A. G. Cullis, L. T. Canham, and P. D. J. Calcott, J. Appl. Phys. **82**, 909 (1997).
[5] L. Skuja, J. Non-Cryst. Solids **239**, 16 (1998).
[6] L. Rebohle, J. von Borany, H. Frob, and W. Skorupa, Appl. Phys. B: Lasers Opt. **71**, 131 (2000).
[7] X. L. Wu, S. J. Xiong, G. G. Siu, G. S. Huang, Y. F. Mei, Z. Y. Zhang, S. S. Deng, and C. Tan, Phys. Rev. Lett. **91**, 157402 (2003).
[8] J. L. Gole, F. P. Dudel, D. Grantier, and D. A. Dixon, Phys. Rev. B **56**, 2137 (1997).
[9] J. L. Gole and D. A. Dixon, J. Phys. Chem. B **101**, 8098 (1997).
[10] J. L. Gole and D. A. Dixon, Phys. Rev. B **57**, 12002 (1998).
[11] L. Pavesi, L. Dalnegro, C. Mazzoleni, G. Franzo, and F. Priolo, Nature (London) **408**, 440 (2000).
[12] M. V. Wolkin, J. Jorne, P. M. Fauchet, G. Allan, and C. Delerue, Phys. Rev. Lett. **82**, 197 (1999).
[13] X. L. Wu, S. J. Xiong, D. L. Fan, Y. Gu, and X. M. Bao, Phys. Rev. B **62**, R7759 (2000).
[14] F. S. Xue, X. M. Bao, and F. Yan, J. Appl. Phys. **81**, 3175 (1997).
[15] Y. H. Zhang, X. J. Li, L. Zheng, and Q. W. Chen, Phys. Rev. Lett. **81**, 1710 (1998).
[16] D. Y. Lee, J. W. Park, J. Y. Leem *et al.*, J. Cryst. Growth **260**, 394 (2004).
[17] C. H. Chen and Y. F. Chen, Appl. Phys. Lett. **75**, 2560 (1999).
[18] L. Tsybeskov, S. P. Duttagupta, and P. M. Fauchet, Solid State Commun. **95**, 429 (1995).
[19] G. G. Siu, X. L. Wu, Y. Gu, and X. M. Bao, J. Appl. Phys. **88**, 3781 (2000).
[20] M. K. Karl and S. R. Rodney, *Fullerenes: Chemistry, Physics, and Technology* (Wiley-Interscience, New York, 2000).
[21] B. Hamilton, J. S. Rimmer, M. Anderson, and D. Leigh, Adv. Mater. (Weinheim, Ger.) **5**, 583 (1992).
[22] L. Zhu and Y. Li, J. Appl. Phys. **77**, 2801 (1995).
[23] S. S. Deng, X. L. Wu, and S. H. Yang, Acta Mater. **52**, 1953 (2004).
[24] D. F. S. Petri, G. Wenz, P. Schunk, and T. Schimmel, Langmuir **15**, 4520 (1999).
[25] Y. H. Xie, W. L. Wilson, F. M. Ross, J. A. Mucha, E. A. Fitzgerald, J. M. Macaulay, and T. D. Harris, J. Appl. Phys. **71**, 2403 (1992).
[26] J. L. Gole, E. Veje, R. G. Egeberg, A. Ferreira da Silva, I. Pepe, and D. A. Dixon, J. Phys. Chem. B **110**, 2064 (2006).
[27] X. Q. Zheng, C. E. Liu, X. M. Bao, F. Yan, H. C. Yang, H. C. Chen, and X. L. Zheng, Solid State Commun. **87**, 1005 (1993).
[28] J. Y. Fan, X. L. Wu, H. X. Li, H. W. Liu, G. G. Siu, and P. K. Chu, Appl. Phys. Lett. **88**, 041909 (2006).
[29] D. Scherrer, Proc. Phys. Soc., London, Sect. A **62**, 741 (1949).
[30] M. C. Bost and J. E. Mahan, J. Appl. Phys. **58**, 2695 (1985).
[31] T. D. Hunt, K. J. Reeson, and R. M. Gwilliam, J. Lumin. **57**, 25 (1993).
[32] N. E. Christensen, Phys. Rev. B **42**, 7148 (1990).
[33] C. Giannini, S. Lagomarsino, F. Scarinci, and P. Castrucci, Phys. Rev. B **45**, 8822 (1992).
[34] P. Zhou, A. M. Rao, K. A. Wang, J. D. Robertson, C. Eloi, M. S. Meier, S. L. Ren, X. X. Bi, P. C. Eklund, and M. S. Dresselhaus, Appl. Phys. Lett. **60**, 2871 (1992).
[35] A. M. Rao, P. Zhou, K. A. Wang *et al.*, Science **259**, 241 (1993).
[36] J. Winter and H. Kuzmany, Solid State Commun. **84**, 935 (1992).
[37] R. A. Jishi, R. M. Mirie, and M. S. Dresselhans, Phys. Rev. B **45**, 13685 (1992).
[38] D. S. Bethune, G. Meijer, W. C. Tang, H. J. Rosen, W. G. Golden, H. Seki, C. A. Brown, and M. S. DeVries, Chem. Phys. Lett. **179**, 181 (1991).